



# Role of dimple textured surface on tribological properties of Ti/Al-codoped diamond-like carbon films

Xiaowei Xu<sup>a,b</sup>, Peng Guo<sup>b</sup>, Leslie Ching Ow Tiong<sup>c</sup>, Xiao Zuo<sup>b</sup>, Xiaowei Li<sup>b,c,\*</sup>, Kwang-Ryeol Lee<sup>c</sup>, Ping Cui<sup>a,b</sup>, Peiling Ke<sup>b,e</sup>, Aiying Wang<sup>b,d,e,\*</sup>

<sup>a</sup> School of Physical Science and Technology, ShanghaiTech University, Shanghai 201210, PR China

<sup>b</sup> Key Laboratory of Marine Materials and Related Technologies, Zhejiang Key Laboratory of Marine Materials and Protective Technologies, Ningbo Institute of Materials Technology and Engineering, Chinese Academy of Sciences, Ningbo 315201, PR China

<sup>c</sup> Computational Science Center, Korea Institute of Science and Technology, Seoul 136-791, Republic of Korea

<sup>d</sup> Ningbo Institute of Industrial Technology, Chinese Academy of Sciences, PR China

<sup>e</sup> Center of Materials Science and Optoelectronics Engineering, University of Chinese Academy of Sciences, Beijing 100049, PR China

## ARTICLE INFO

### Keywords:

Diamond-like carbon  
Surface texturing  
Area density  
Tribological property  
Hybrid ion beam technique

## ABSTRACT

Surface textured diamond-like carbon (DLC) films with Ti and Al dopants (Ti/Al-DLC) were fabricated by a two-step process, including the photo- and anisotropic-etching of silicon substrate for micro-dimple texturing and the hybrid ion beam deposition for Ti/Al-DLC film. The role of different dimple-textured area densities (0~40%) on the tribological behavior of Ti/Al-DLC film was mainly investigated; the corresponding surface topographies and atomic bond structure of intrinsic films, wear tracks, and wear scars were evaluated systematically to disclose the fundamental mechanism. Results revealed that the dimple-textured structure on film surface had a significant effect on the tribological property of Ti/Al-DLC film rather than the microstructure and mechanical performances. Compared to the untextured Ti/Al-DLC film, the case with dimple-textured area density of 5% exhibited the reduction in coefficient of friction by 17.8% and in wear rate by 44.5%, respectively. This attributed to the synergistic effect of the tribo-induced graphitization and the capturing efficiency of micro-dimples to the wear particles. However, with further increasing the textured area density from 5% to 40%, the locally high contact pressure resulted in the lack of graphitization and the increase of roughness at the friction interface, which prohibited the sliding of friction interface following the weakened tribological property.

## 1. Introduction

Diamond-like carbon (DLC) film exhibits the hard hardness, corrosion resistance, superior tribological and optical properties, which has served as a protective coating for multitudinous applications, such as aviation [1,2], automotive components [3–5], micro-nano electric mechanical systems [6–8], and other engineering fields [9,10]. Nevertheless, in order to further enhance the tribological properties of DLC film and extend its lifetime and reliability for practical applications, many efforts have been conducted to tailor the DLC structure, such as metal doping, surface modification, surface texturing, etc. As mentioned, co-doping two metal elements into the carbon matrix is one of the effective approaches to endow the DLC film with both the outstanding mechanical and tribological properties [11–13]. For example, Zhou et al. [14] proved that the duplex doped nc-WC/a-C(Al) nanocomposite film possessed an appropriate combination of high hardness,

superior low-friction, and anti-wear performances. In addition, Kong et al. [15] reported the DLC films co-doped by Ti/Al elements, which possessed the superior mechanical property along with the low coefficient of friction (COF, ~0.05).

Surface texturing also attracts extensive attention due to its special functions, which can act as a structural design to play an important role in realizing the improvement of tribological performance. The micro- and nano-textured structures can serve as reservoirs to retain the wear grindings that are generated at the mated friction interface. This minimizes the third-body abrasion to extend the lifetime of coated surface. At present, many studies have focused on the optimization of geometric patterns (groove [16], square [17], crisscross [18], dimple [19]), area density, diameter, and depth of textured structures to realize the improvement of tribological property in synergism. For example, Aoki et al. [20] demonstrated that the segment-structured DLC film had a low coefficient and a significant reduction in wear rate compared with

\* Corresponding authors.

E-mail addresses: [lixw0826@gmail.com](mailto:lixw0826@gmail.com) (X. Li), [aywang@nimte.ac.cn](mailto:aywang@nimte.ac.cn) (A. Wang).

<https://doi.org/10.1016/j.tsf.2020.138136>

Received 7 January 2020; Received in revised form 13 May 2020; Accepted 21 May 2020

Available online 29 May 2020

0040-6090/ © 2020 Elsevier B.V. All rights reserved.

the continuous DLC due to the influence of the segment structure on the elastic deformation of the substrate as well as the stress relaxation of film. Arslan et al. [21] found that for DLC films, the optimal diameter and depth of textured structure mainly depended on the contact pressure during the friction process for the non-conformal contact. But Ronen et al. [22] reported that the dimples could improve the tribological performance for the conformal contacts, when the aspect ratio (the ratio of dimple depth to dimple diameter) was 0.1-0.18. Kashyap et al. [23] also demonstrated that the micro-groove texture width was critical for obtaining the maximum tribological benefits under the bio-lubricating condition. Wu et al. [24] emphasized the key role of textured density in improving the friction coefficient and wear resistance.

In previous studies [15,25–27], we have prepared the Ti/Al co-doped DLC (Ti/Al-DLC) films with high performance using the hybrid ion beam (HIB) deposition system and systematically clarified the relationship between deposition parameters and tribological properties of DLC films induced by Ti/Al co-doping. However, the synergistic effect of Ti/Al co-doping and surface texturing on the tribological behaviors of DLC films is still not understood yet, which is requisite to tailor the DLC structure and improve its durability and reliability for engineering applications. Hence, in the present work, we fabricated the Ti/Al-DLC films with surface dimple-textured structures. Combined with the analysis of microstructure, surface topography, mechanical properties, and bonding state, the effect of different textured area densities (0–40%) on the tribological property of Ti/Al-DLC film was mainly investigated to explore the underlying friction mechanism of DLC film.

## 2. Experimental details

### 2.1. Preparation of Ti/Al-DLC films with surface texturing

A two-step process, consisting of photo- and anisotropic-etching of silicon substrate for micro-dimple texturing and the HIB deposition for Ti/Al-DLC film, was designed to fabricate the Ti/Al-DLC films with surface texturing, as illustrated in Fig. 1. First, micro-dimple textured surface patterns with different area densities (5%, 20%, 30%, and 40%) were acquired on the silicon P (100) monocrystalline wafers by the photo- and anisotropic-etching processes using inductively coupled plasma etching system. The diameter and depth of each dimple structure on Si substrate were 20  $\mu\text{m}$  and 0.8  $\mu\text{m}$ , respectively, with a tolerance of  $\pm 5$ -10%; the parietal wall was inclined with an angle of  $\sim 70^\circ$  from the bearing surface. After that, the Ti/Al-DLC films were deposited on the textured silicon wafers using the HIB deposition system. This system was composed of a linear anode-layer ion source (ALIS) and a DC magnetron sputtering source (DCMS), in which the ALIS was provided with  $\text{C}_2\text{H}_2$  gas for DLC deposition and the DCMS was supplied with a Ti/Al composite target for Ti/Al co-doping.

Prior to the Ti/Al-DLC deposition process, the textured silicon

substrates were ultrasonically cleaned using acetone and ethyl alcohol for 20 minutes, respectively, and dried using nitrogen flow. Then, these pre-treated substrates were put into the vacuum chamber with a base pressure of about  $2.7 \times 10^{-3}$  Pa, in which the distances between substrates and ALIS or sputtering target were fixed at 20 cm separately. After that, the plasma etching with  $\text{Ar}^+$  bombardment was conducted at a bias voltage of  $-100$  V to remove the contamination and impurities from the substrate surface. During the deposition process, the Ti/Al interlayer and Ti/Al-DLC film were subsequently deposited on the substrate and the corresponding process parameters were shown in Table 1. The details for film deposition process could be found in our previous study [15]. For convenience, the as-deposited films with textured area densities of 0%, 5%, 20%, 30%, and 40% were abbreviated as D0, D5, D20, D30, and D40, respectively.

### 2.2. Microstructure characterization

The film thickness was recorded by the profilometer (Alpha-Step IQ) through the needle tip sweeping the shadow mask between as-deposited film and bare substrate. The carbon atomic bond structure of as-deposited films and wear tracks were characterized by Raman spectroscopy (Renishaw, inVia-reflex). Furthermore, the cross-sectional and surface morphologies of the films were observed through field emission scanning electron microscope (FEI Quanta FEG250). The three-dimensional (3D) topographies of films and wear tracks were characterized by the laser scanning confocal microscopy (LSCM, Zeiss LSM700) and scanning probe microscope (SPM, Dimension 3100).

### 2.3. Mechanical and tribological tests

The hardness and Young's modulus of deposited films were determined through Nanoindenter (MTS-G200) with a continuous stiffness mode; the maximum indentation depth equaled to the 1/10 thickness value of as-deposited film to eliminate the substrate influence. The tribological tests were performed on the pin-on-disk tribometer (Anton Paar, TRB<sup>3</sup>) under atmosphere environment of a relative humidity of  $40 \pm 5\%$  and a temperature of  $25 \pm 5^\circ\text{C}$ . The GCr15 steel ball (HRC60) with a diameter of 6 mm was used as counter body. Each measurement was set to 6000 laps with the rotating speed of 320 rpm, a radius of 1.5 mm, and a normal load of 5 N. Three replicated tests were undertaken to calculate the average COF ( $\mu$ ) and wear rate ( $W$ ). The wear rate was calculated using the Archard equation:

$$W = \frac{V}{L \times N} \quad (1)$$

where  $W$ ,  $L$ , and  $N$  are defined as the wear rate, total sliding distance, and normal load, respectively;  $V$  represents the wear volume loss, which is calculated by the integral of cross-sectional wear track profile.

## 3. Result and discussion

### 3.1. Microstructure

Fig. 2a and b illustrate the 2D and 3D morphologies of Ti/Al-DLC films with different dimple-textured area densities. Note that for each case, the textured surface of film is composed of parallel micro-patterned dimples with the diameter of 20  $\mu\text{m}$  and depth of  $\sim 1.2$   $\mu\text{m}$ , corresponding to the aspect ratio of 0.06 which is less than 0.1 [21]. With increasing the textured area density from 5% to 40%, the distance between the center of adjacent micropores decreases from about 80 to 28  $\mu\text{m}$  (insets of Fig. 2a), which is accompanied by the increased surface roughness from 4.8 to 67.6 nm.

Regarding the cross-sectional morphology, Fig. 3a shows that the D0 sample consists of a Ti/Al-DLC film with thickness of  $\sim 1.84$   $\mu\text{m}$  and a Ti/Al interlayer with thickness of  $\sim 0.6$   $\mu\text{m}$ , in which the interlayer presents a compact columnar-grained crystalline structure. However,

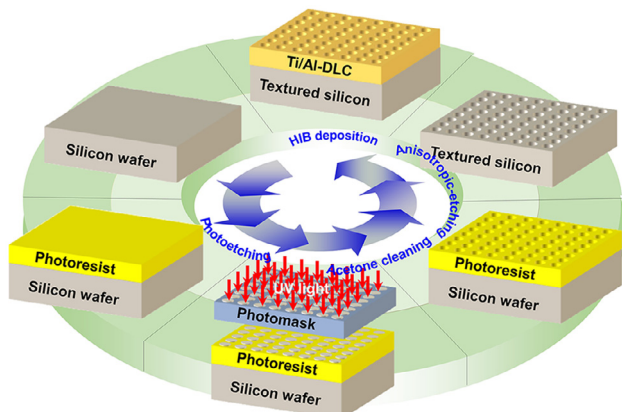


Fig. 1. Preparation process of the Ti/Al-DLC films with surface texturing.

**Table 1**  
Deposition parameters for the Ti/Al interlayer and Ti/Al-DLC films.

	Sputtering current /A	Ar flow /sccm	LIS working current /A	LIS working voltage /V	Hydrogenated gas	Hydrogenated gas flow / sccm	Bias voltage /V	Working pressure /Pa	Deposition time /min
Ti/Al interlayer	4	55	/	/	/	/	-100	0.43	16
Ti/Al-DLC	2.5	70	0.2	1400 ± 50	C <sub>2</sub> H <sub>2</sub>	10	-50	0.56	60

for these textured samples, similar thickness values to the D0 sample are obtained, as illustrated in Fig. 3b. This indicates that by processing the substrate to fabricate the textured film, the change of area density

has no effect on the dynamic growth of Ti/Al-DLC film. In addition, for each case, the doped Ti and Al contents are  $6.31 \pm 0.31$  and  $8.07 \pm 0.42$  at.%, respectively, which are also independent of the

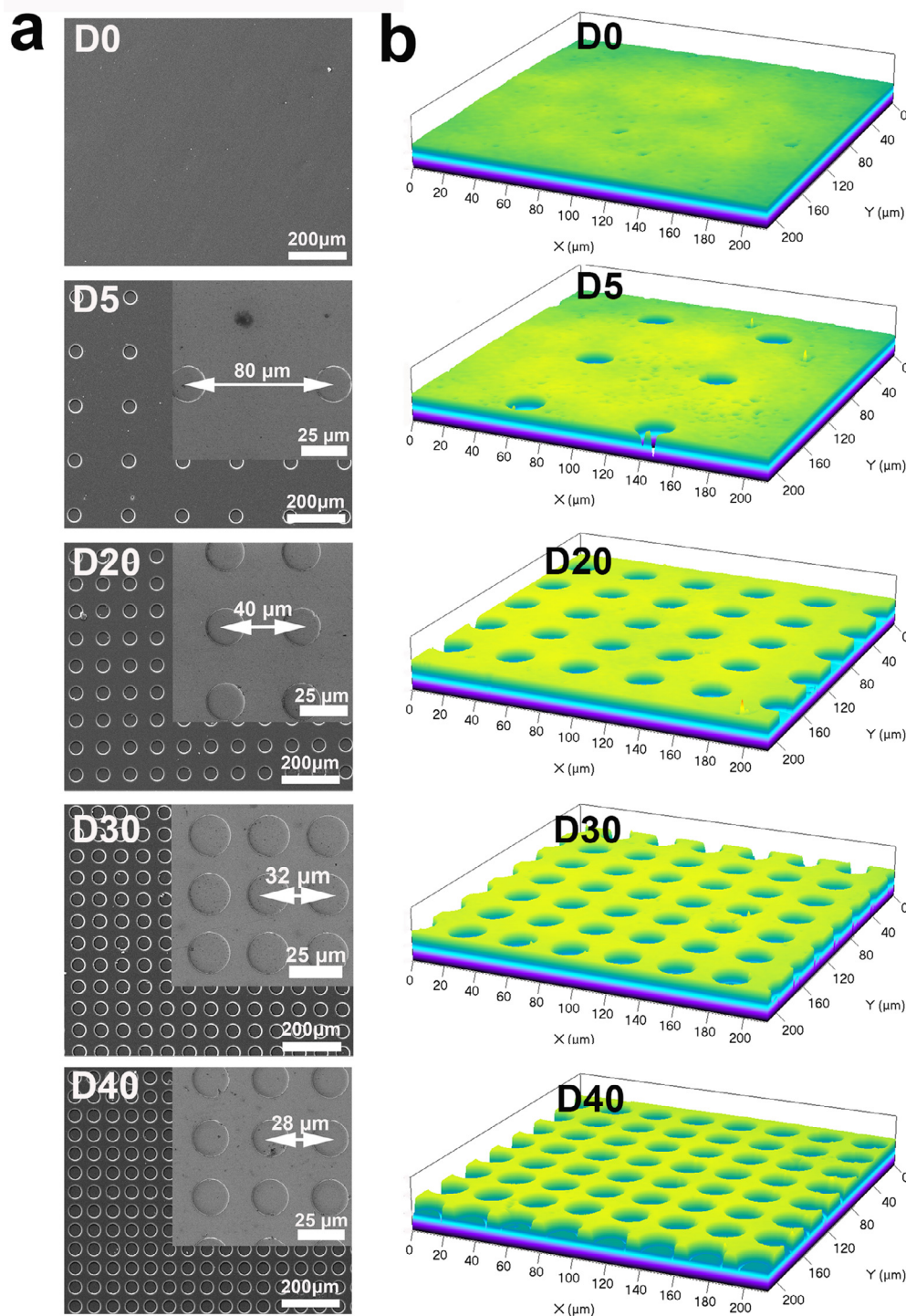


**Fig. 2.** (a) 2D and (b) 3D morphologies of untextured and textured Ti/Al-DLC films with different textured area densities (5%~40%).

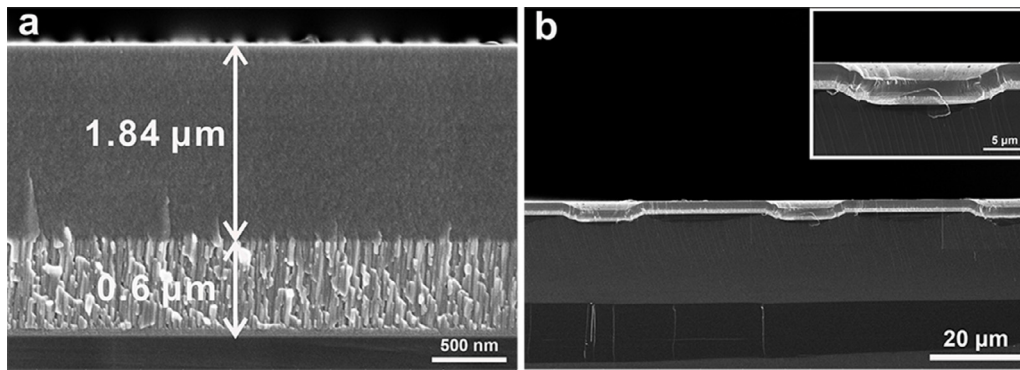


Fig. 3. Cross-sectional morphologies of (a) untextured and (b) textured films. The inset is the magnified microscopic image of dimple structure.

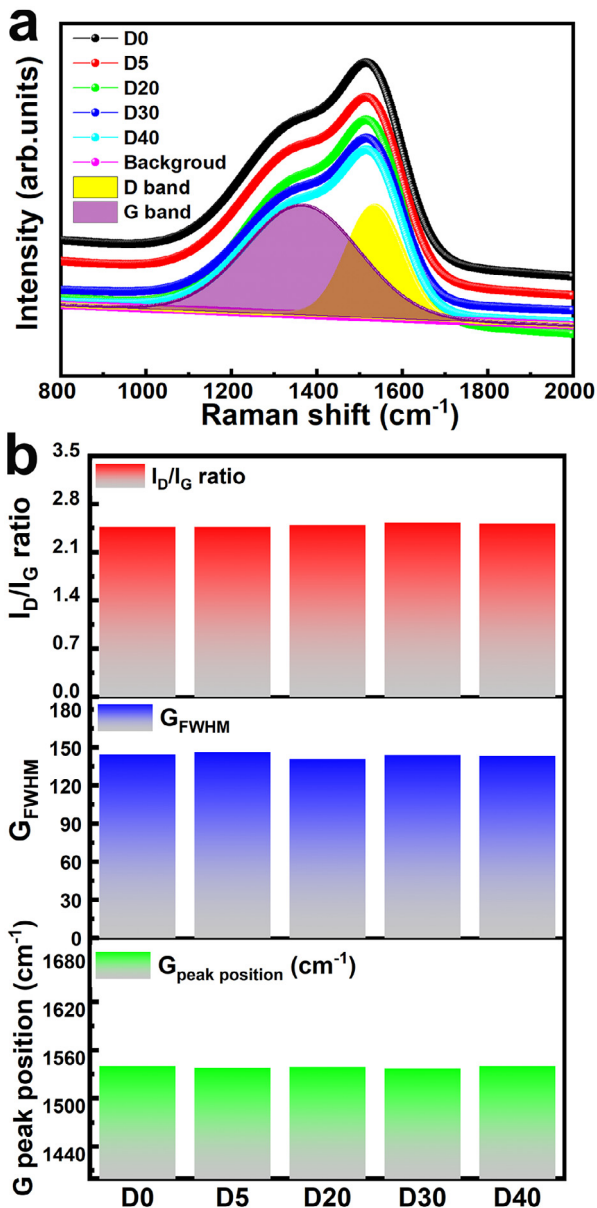


Fig. 4. (a) Raman spectra and (b) fitting results including  $I_D/I_G$ ,  $G_{FWHM}$ , and G peak position of the Ti/Al-DLC films with different dimple-textured area densities.

textured area density.

Raman spectroscopy is further implemented to characterize the change of carbon atomic bond structure of DLC film induced by surface texturing, as illustrated in Fig. 4. For each film, the spectrum can be fitted into two broad peaks, which are located at  $1345\text{ cm}^{-1}$  (D band) and  $1535\text{ cm}^{-1}$  (G band), respectively. This is the typical character of amorphous carbon structure [28,29]. In particular, the intensity ratio of D peak to G peak ( $I_D/I_G$ ), the full width at the half maximum of G peak ( $G_{FWHM}$ ), and the G peak position are calculated to check the structural evolution of intrinsic carbon structure with textured area density, as shown in Fig. 4b. It can be found that with the textured area density increased from 0% to 40%, the  $I_D/I_G$ ,  $G_{FWHM}$ , and G peak position almost remain constant values. These indicate that the microstructure of Ti/Al-DLC film does not rely on the dimple-textured area density, implying the same mechanical property as the untextured case.

### 3.2. Mechanical property

Fig. 5a shows the indentation curves of untextured Ti/Al-DLC film, which is also similar to the cases with surface texturing conditions. With increasing the indentation depth from 0 to the 1/10 thickness value of as-deposited specimen [30], the hardness (H) and elastic modulus (E) decrease first and then become stable at the values of about 14.8 and 175.6 GPa, respectively. The average hardness and modulus values, which are obtained from the stable stage in Fig. 5a, are used to quantify the effect of different textured area densities on the mechanical property, as given in Fig. 5b, in which the error bars represent the standard deviation errors from six indentations. It exhibits the negligible changes of hardness and elastic modulus with textured area density, which coincide with the Raman analysis (Fig. 4). Moreover, Fig. 5c provides the  $H/E$  and  $H^3/E^2$  ratios, which closely correlate with the durability and plastic deformation resistance of the films, respectively [31, 32]. They also show slight fluctuation when the film ranges from D0 to D40, further indicating the independence of mechanical property from dimple-textured area density.

### 3.3. Tribological performance

The friction curves of untextured and textured Ti/Al-DLC films with different textured area densities are illustrated in Fig. 6a. The steady-state COF value is displayed in Fig. 6b for each film, which is the average value of three friction tests. Compared to the untextured Ti/Al-DLC film (0.095), the COF value (0.078) is reduced by 17.8% when the dimple-textured area density is 5%. However, with further increasing the textured area density to 20%, 30%, and 40%, the COF increases obviously and then decreases; the maximum COF value, 0.145, is obtained for the D20 film. In particular, Fig. 6 shows that there is no monotonous relationship between COF value and textured area density (0~40%). This indicates that the dimple-textured area density could play positive or negative effect on the tribological performance of Ti/

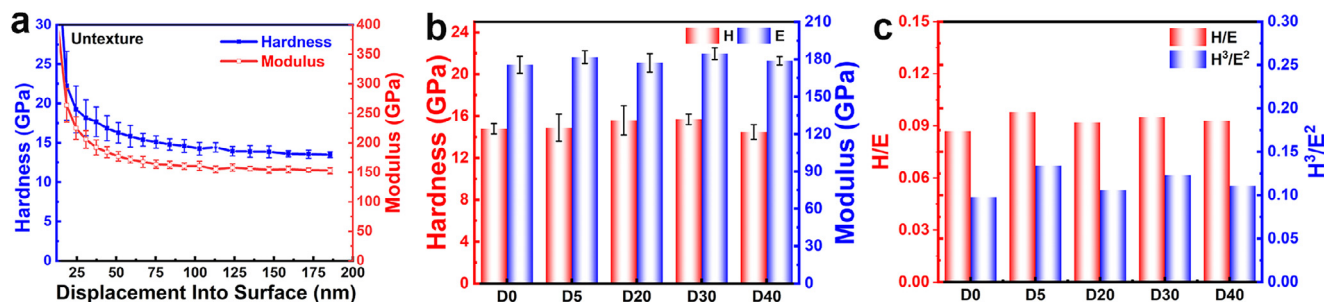


Fig. 5. Change of the mechanical property of Ti/Al-DLC films with surface textured area density. (a) Indentation curves of untextured Ti/Al-DLC film (D0); (b) average hardness and elastic modulus; (c) H/E and  $H^3/E^2$  ratios.

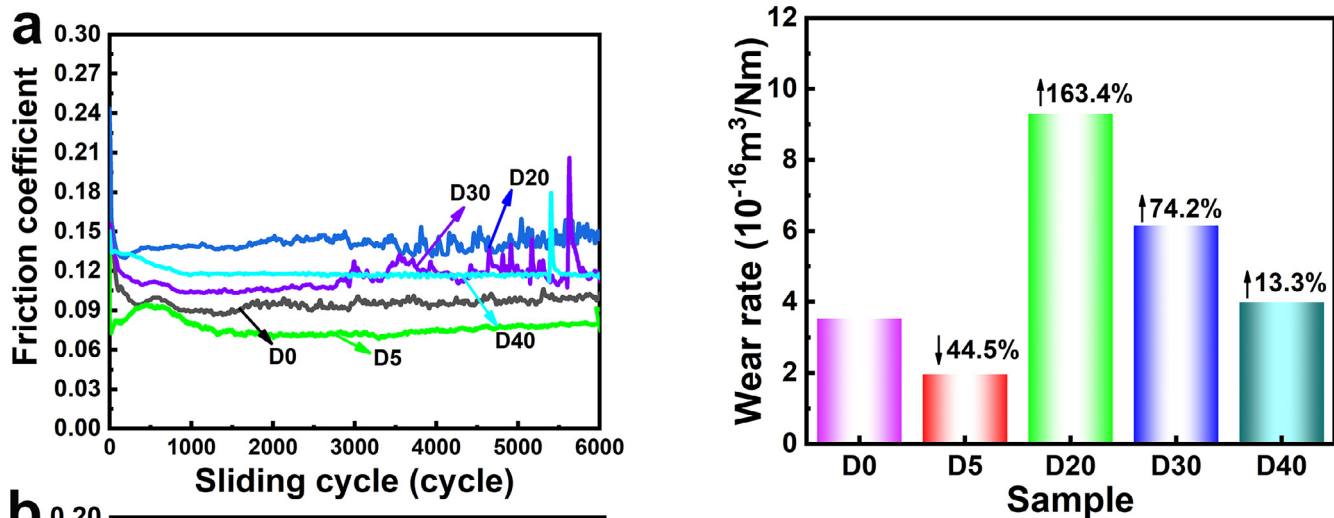


Fig. 7. Wear rates of the untextured and textured Ti/Al-DLC films with different dimple-textured area densities.

Fig. 6. (a) Friction curves and (b) average COF values of the untextured and textured Ti/Al-DLC films with different dimple-textured area densities. The error bars represent the standard deviation errors from the average of three friction tests.

Al-DLC film and also induces the transformation of underlying friction mechanism, as will be discussed later. In addition, the friction curve of untextured film reaches the stable friction stage after a short running-in period (~500 cycles), but the films with high dimple-textured area densities undergo long running-in processes following drastic fluctuations, which results from the non-uniform distribution of wear debris and the increased surface roughness.

According to Eq. (1), the wear rates of Ti/Al-DLC films are calculated, as presented in Fig. 7. As can be seen that the D5 film also exhibits a superior anti-wear behavior, which is about 44.5% lower than the untextured case. When the dimple-textured area density is increased

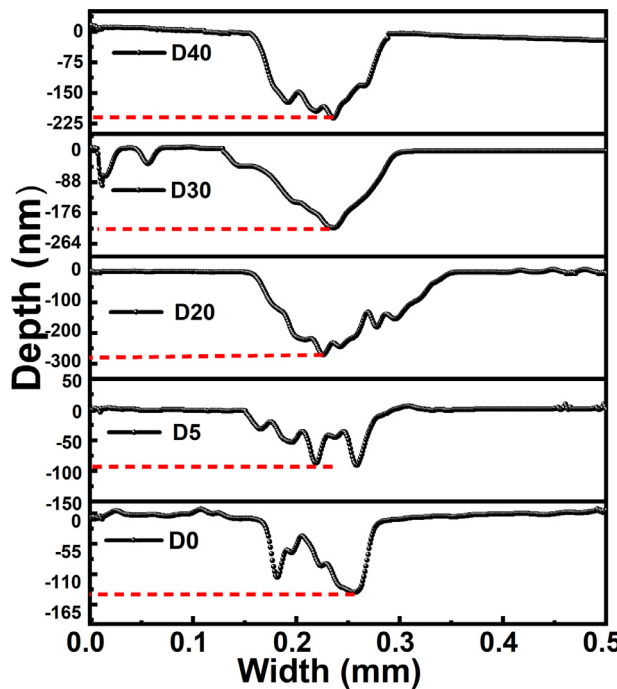
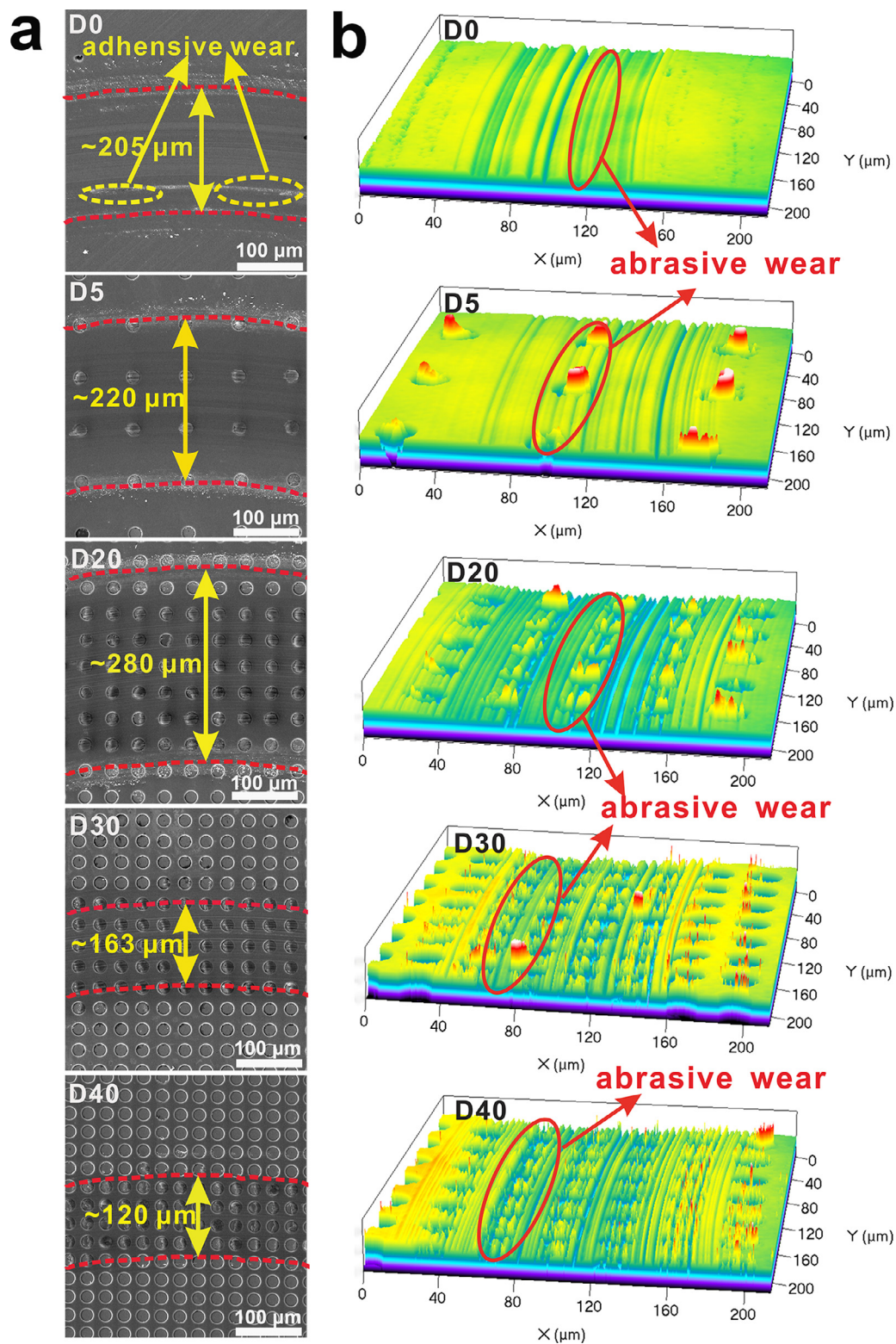


Fig. 8. Cross-sectional profiles of wear tracks of the untextured and textured Ti/Al-DLC films after friction tests.



**Fig. 9.** (a) 2D surface topographies and (b) corresponding non-contact 3D surface profiler images of wear tracks of the untextured and textured Ti/Al-DLC films after friction tests.

to 20%, the wear rate presents a significant increase, which is about 163.4% higher than that of the D0 film, being consistent with the change of COF value in Fig. 6b. However, with the dimple area density further increased to 30% and 40% from 20%, the wear rate shows a decreasing trend, which is still higher than that of the D0 film. This change of wear rate may be related to the texturing-induced increase of

actual contact pressure at the sliding interface, as will be discussed later.

In order to shed light on the underlying friction and wear mechanisms induced by different dimple-textured area densities, Figs. 8 and 9 present the cross-sectional profiles, corresponding non-contact 3D surface profiler images, and 2D surface topographies of wear tracks

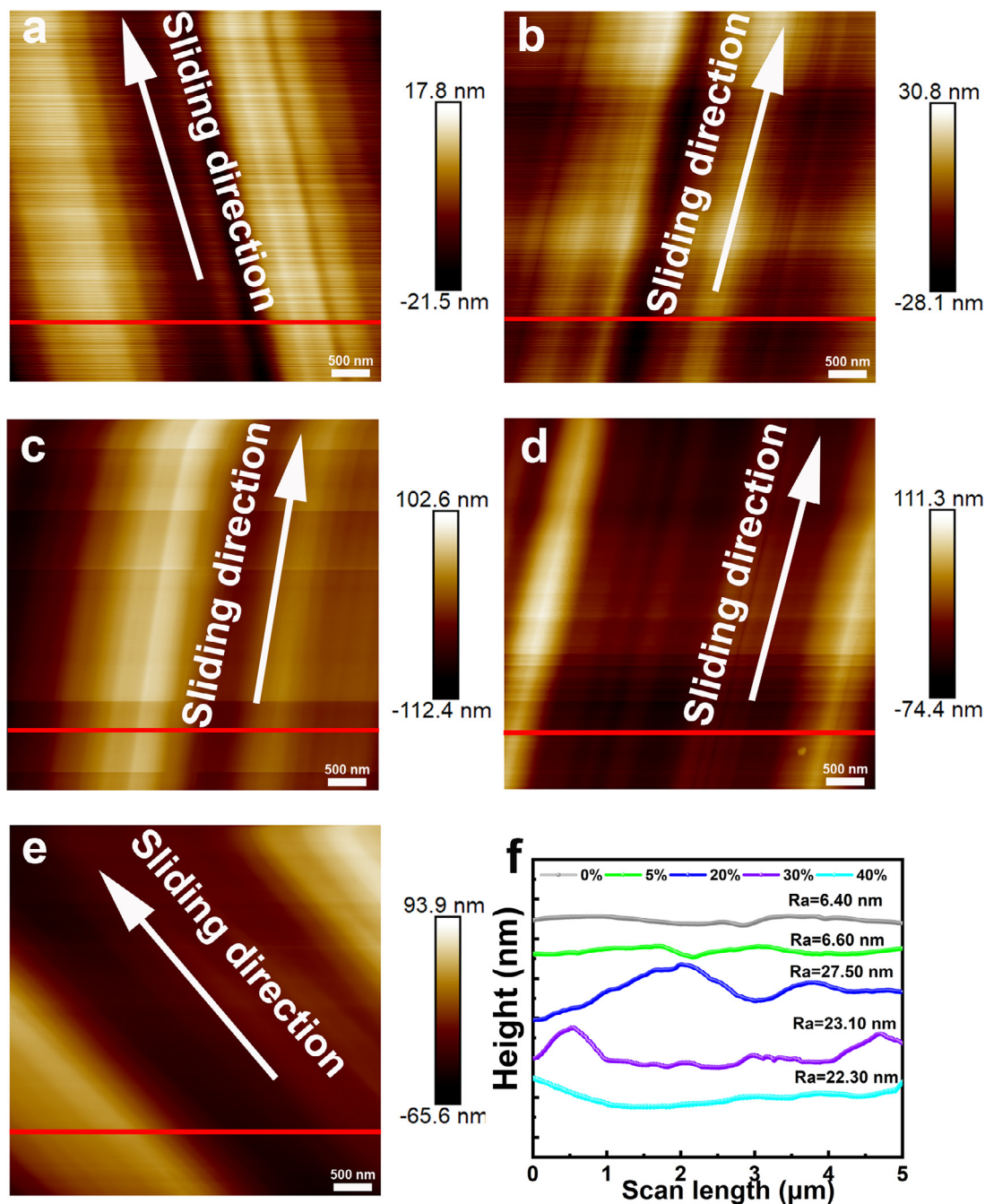


**Fig. 10.** AFM morphologies of the worn surface of (a) D0, (b) D5, (c) D20, (d) D30, and (e) D40 Ti/Al-DLC films and (f) their corresponding line profiles, in which the red horizontal lines are illustrated in 2D AFM morphologies on behalf of the locations where the profiles are collected.

of the untextured and textured Ti/Al-DLC films after friction tests. For the case of D0 film, the depth and width of wear track are 140 nm and 205  $\mu\text{m}$ , respectively (Figs. 8 and 9a); some plough grooves exist in the worn surface (Fig. 9b), indicating the presence of abrasive wear during the friction process. In addition, the wear trace of D0 film, which is smooth and shallow, conserves an amount of wear debris and micro-particles (Fig. 9a), suggesting the extra contribution from adhesive wear. When the dimple-textured area density is 5% (D5), the wear width increases to 220  $\mu\text{m}$  (Fig. 9a), but the wear track presents a significant drop in wear depth to only 90 nm, which corresponds to the low wear rate shown in Fig. 7. In particular, note that these dimples can capture the wear debris generated during the sliding process and thus lubricate or smooth the sliding interface (Fig. 9a and the region with red color in Fig. 9b). So the surface roughness of D5 wear track (6.60

nm) almost has no change compared to that of D0 film (6.40 nm), as illustrated in Fig. 10. Although the presence of dimples leads to the increase of initial surface roughness, the storage effect of dimples on abrasive debris reduces the surface roughness and the corresponding contact pressure around dimple positions, contributing to the drop of friction and wear for the D5 textured sample. These results ensure that a proper textured morphology facilitates the improvement of wear resistance of DLC film.

However, with the further increase of textured area density to 20%, both the depth and width of wear track reach the maximal values of 270 nm (Fig. 8) and 280  $\mu\text{m}$  (Fig. 9a) separately, corresponding to the high wear rate (Fig. 7). Although increasing the number of dimples can store more wear debris, it also reduces the bearing capacity of film due to the discontinuity of the matrix. In particular, the increase of textured area

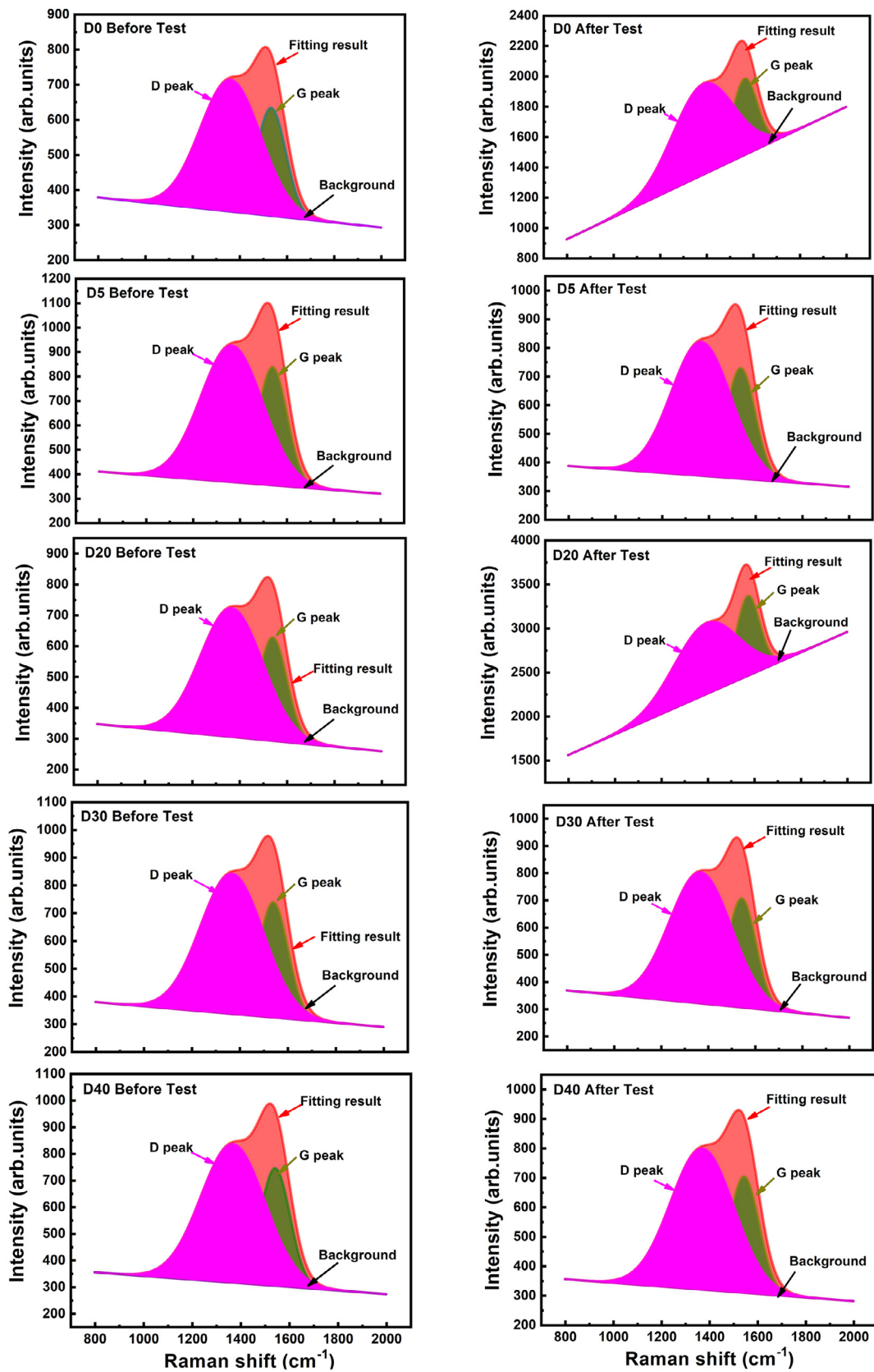


Fig. 11. Comparison of Raman spectra of the wear tracks before and after friction tests for each case.

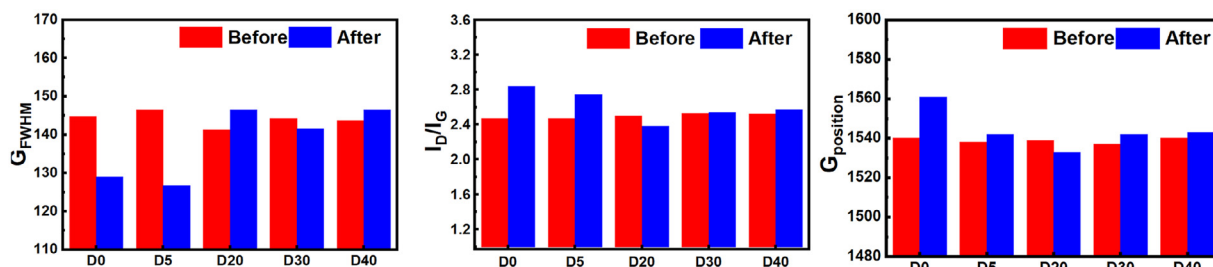


Fig. 12. Fitting results of Raman spectra of wear tracks before and after friction tests, including G peak position,  $G_{FWHM}$ , and  $I_D/I_G$ .

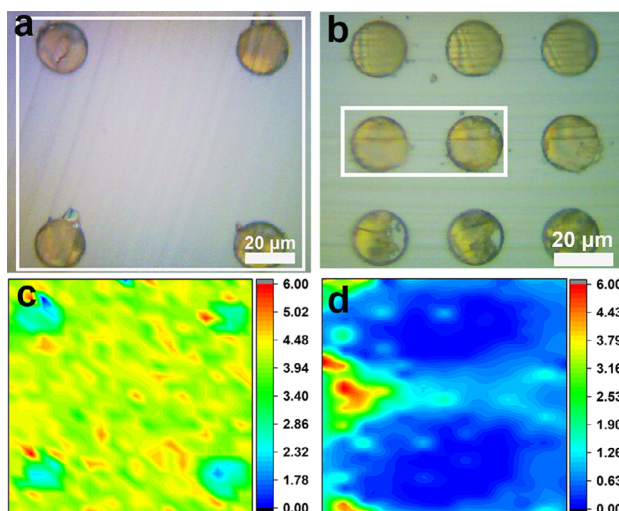


Fig. 13. Optical morphologies of wear tracks of (a) D5 and (b) D20 films; (c) and (d) are the corresponding Raman mapping images of worn surface marked with white rectangles of D5 and D20 films, respectively, and the intensity of the signal was between 800 and 2000  $cm^{-1}$ .

density not only reduces the real contact area of sliding interface to a certain extent following the increased Hertzian contact pressure [33,34], but also aggravates the surface roughness obviously to prohibit the sliding of friction interface. As a result, the wear behavior is accelerated (Fig. 7) and the obvious micro-cutting and plough grooves appear in a short-term friction process. This result is also confirmed by the AFM analysis of D20 film, which shows the highest roughness of 27.50 nm than other cases (Fig. 10).

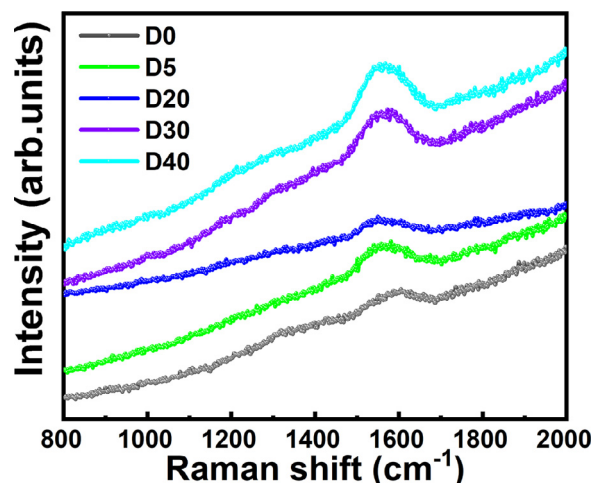


Fig. 15. Raman spectra of wear scars of Ti/Al-DLC films with different textured area densities.

While the textured area density reaches 30% (D30) and 40% (D40), the widths of wear tracks drastically decrease to 163 and 120  $\mu m$ , respectively. The initial surface roughness values with textured area density also increase to 57.7 nm for D30 and 67.6 nm for D40 significantly, raising the sliding barrier of mated surface. However, these textured dimples can also effectively capture the wear debris during the friction process (Fig. 9) to smooth the sliding interface and weaken the negative effect of interfacial roughness on friction, contributing to the drop of COF and wear rate. This is confirmed by the decreased roughness values of wear tracks in Fig. 10. In addition, the worn

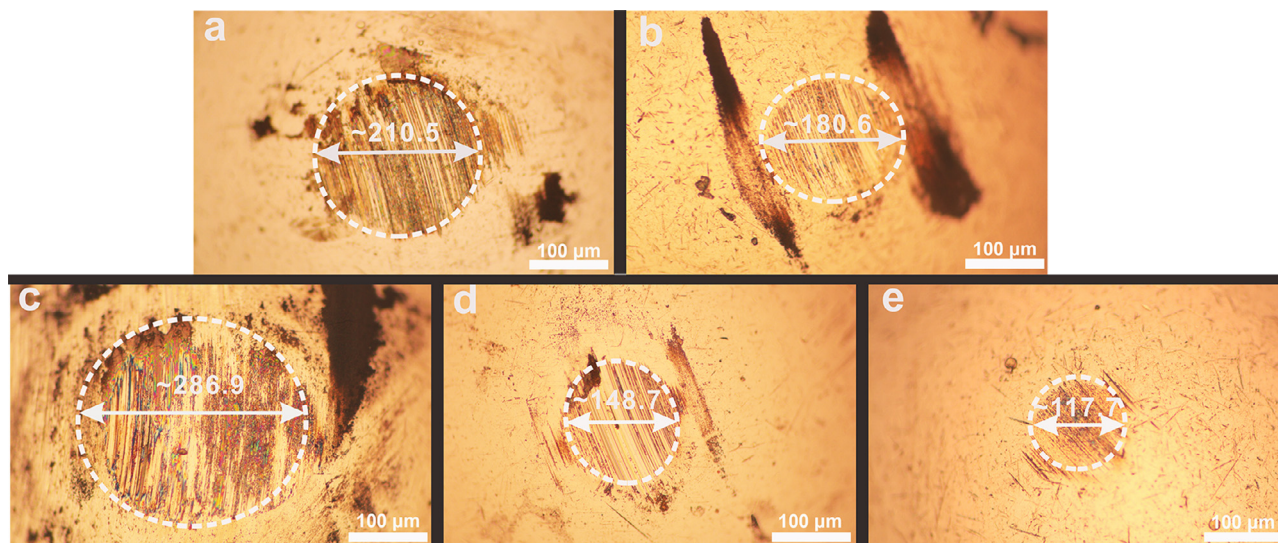


Fig. 14. Optical morphologies of wear scars on mating balls sliding against (a) D0, (b) D5, (c) D20, (d) D30, and (e) D40 Ti/Al-DLC films, respectively.

surfaces exhibit different levels of deep furrows and abrasive wear, as shown in Fig. 9b, while there has no obvious adhesive wear occurred during the friction process for the textured films and also no delamination or brittle cracking observed in the wear tracks of all films.

Moreover, Raman spectroscopy of Ti/Al-DLC films before and after friction tests are recorded separately to distinguish the change of carbon bond structure of wear tracks, as shown in Fig. 11. The quantitative fitting results are illustrated in Fig. 12. Compared to the Raman results of films obtained before the friction process, the D0 and D5 films after friction process exhibit the positive deviations of G peak positions and  $I_D/I_G$  values following the decrease of  $G_{FWHM}$ . This indicates the transformation of carbon hybridized structure from  $sp^3$  to  $sp^2$ , namely graphitization transition [35,36], which can reduce the shearing barrier to the sliding interface and thus play a synergistic effect with the debris capturing ability to lower the COF value for D5 film. It is in consistence with previous literature reported by Arslan et al. [21]. However, for D20, D30, and D40 films, the G peak position and  $I_D/I_G$  ratio only have slight changes (Fig. 12), implying that the surface texturing could dramatically affect the generation of graphitization during the friction process. To thoroughly analyze the insight into friction, Raman mappings on the worn surfaces with sizes of  $120\ \mu\text{m} \times 100\ \mu\text{m}$  for D5 film and  $60\ \mu\text{m} \times 40\ \mu\text{m}$  for D20 film are carried out, respectively, with the characteristic Raman shift at  $1400\ \text{cm}^{-1}$ , as shown in Fig. 13. First, there is no significant tribo-film existed outside the dimples for both the D5 and D20 films (Fig. 13a and b). However, Raman mapping images clearly illustrate the intensity of  $I_D/I_G$  at different positions, revealing that compared to the D20 film (Fig. 13d), the D5 film shows a homogeneous graphitization at the sliding interface (Fig. 13c), which contributes to the improvement of friction behavior.

Furthermore, the optical morphologies of wear scars on the mating balls are characterized, as illustrated in Fig. 14. After the friction process, although a transfer film is formed on the mating ball surface for each case, as confirmed by the Raman spectroscopy in Fig. 15, it has an inhomogeneous and loose structure instead of a dense and compact state as reported by Li et al. [15]. Therefore, this transfer film plays a limited role to prevent the direct contact between film and counterpart and to reduce the shearing strength [37]. However, it should be mentioned that compared to the untextured case, the application of surface texturing can hinder the formation of transfer film [38]. This attributes to the texturing-induced decrease of real contact area, bringing the local enlargement of contact pressure at the edges of micropores. In addition, similar to the results reported by Zhou et al. [25], Ti and Al dopants also make no contribution to the friction behavior in the present work. Therefore, based on the systematical analysis of wear track and wear scar, the effect of different textured area density on the friction behavior of Ti/Al-DLC film originates from the complicated factors, including the wear debris storage in dimple (Fig. 9), roughness of contact surface (Fig. 10), graphitization of wear track (Figs. 12 and 13).

#### 4. Conclusions

Ti/Al-DLC films with different micro-dimple area densities (0%, 5%, 20%, 30%, and 40%) were prepared using the combined approach, including the substrate pre-texturing by photo- and anisotropic-etching and the film deposition by HIB system. The microstructure, mechanical, and tribological performances of untextured and textured films were systematically explored to unveil the relationship between structural properties and textured area density. Results revealed that the existence of surface texturing had no effect on the microstructure and mechanical performance of Ti/Al co-doped DLC films. However, compared to the untextured Ti/Al-DLC film, the film with dimple-textured area density of 5% exhibited a stable friction tendency and the COF and wear rates values were decreased by 17.8% and 44.5%, respectively. This resulted from the synergistic effect of the graphitization of friction interface and the capturing efficiency of micro-dimple to wear particles, reducing the shearing strength of sliding interface. But with further increasing the

textured area density to 20%, 30%, and 40%, the COF and wear rate increased. When the textured area density was 20%, the COF and wear rate values were maximally increased by 52.6% and 163.4%, respectively, by comparing to the untextured case. This was not only attributed to the absence of interfacial graphitization, but also contributed by the significant increase of roughness induced by the high contact pressure at the contact interface. In addition, the doped Ti/Al dopants and transfer layer presented slight effect on the friction behavior of Ti/Al-DLC film. The present work discloses the relationship between tribological properties of the Ti/Al-DLC films and surface textured area density, which could guide the effective surface/interface modulation of DLC structure for engineering applications.

#### CRedit authorship contribution statement

**Xiaowei Xu:** Conceptualization, Data curation, Formal analysis, Methodology, Investigation, Visualization, Writing - original draft. **Peng Guo:** Formal analysis, Methodology, Investigation, Writing - original draft. **Leslie Ching Ow Tiong:** Formal analysis, Writing - original draft. **Xiao Zuo:** Formal analysis, Writing - original draft. **Xiaowei Li:** Conceptualization, Data curation, Funding acquisition, Investigation, Resources, Supervision, Writing - original draft, Writing - review & editing. **Kwang-Ryeol Lee:** Writing - review & editing, Funding acquisition. **Ping Cui:** Writing - review & editing, Funding acquisition. **Peiling Ke:** Writing - review & editing, Funding acquisition. **Aiying Wang:** Conceptualization, Supervision, Writing - review & editing, Funding acquisition, Resources.

#### Declaration of Competing Interest

None.

#### Acknowledgments

This research was supported by the National Natural Science Foundation of China (51772307), National Science and Technology Major Project (2017-VII-0012-0108), A-class pilot of the Chinese Academy of Sciences (XDA22010303), Ningbo Science and Technology Innovation Project (2018B10014), and the Korea Research Fellowship Program funded by the Ministry of Science and ICT through the National Research Foundation of Korea (2017H1D3A1A01055070).

#### References

- [1] A. Grill, Diamond-like carbon coatings as biocompatible materials—an overview, *Diam. Relat. Mater.* 12 (2003) 166–170.
- [2] P.F. Macário, A. Vieira, L. Manfro, M.G.P. da Silva, P. Leite, L. Vieira, Corrosion behavior of Al2024-T3, Al5052-H32, and Al6061-T6 aluminum alloys coated with DLC films in aviation fuel medium, *Jet A-1 and AVGAS 100LL*, *Mater. Corros.* 70 (2019) 2278–2291.
- [3] M.M. Quazi, M.A. Fazal, A.S.M.A. Haseeb, F. Yusof, H.H. Masjuki, A. Arslan, Laser-based surface modifications of aluminum and its alloys, *Crit. Rev. Solid State Mater. Sci.* 41 (2015) 106–131.
- [4] J. Huang, L. Wang, B. Liu, S. Wan, Q. Xue, In vitro evaluation of the tribological response of Mo-doped graphite-like carbon film in different biological media, *ACS Appl. Mater. Interfaces* 7 (2015) 2772–2783.
- [5] A. Choleridis, S. Sao-Joao, J. Ben-Mohamed, D. Chern, V. Barnier, G. Kermouche, C. Heau, M.-A. Leroy, J. Fontaine, S. Descartes, C. Donnet, H. Klöcker, Experimental study of wear-induced delamination for DLC coated automotive components, *Surf. Coat. Technol.* 352 (2018) 549–560.
- [6] M.R. Price, B. Raeymaekers, Quantifying adhesion of ultra-thin multi-layer DLC coatings to Ni and Si substrates using shear, tension, and nanoscratch molecular dynamics simulations, *Acta Mater.* 141 (2017) 317–326.
- [7] M.R. Solouk, M.H. Shojaeefard, M. Dahmard, Parametric topology optimization of a MEMS gyroscope for automotive applications, *Mech. Syst. Sig. Process.* 128 (2019) 389–404.
- [8] W. Wang, L. Ji, H. Li, H. Zhou, P. Ju, J. Chen, Enhancing field electron emission behavior and mechanical properties of hydrogenated amorphous carbon films by incorporating vertically aligned carbon nanowires via facile reactive magnetron sputtering, *J. Alloys Compd.* 784 (2019) 463–470.
- [9] G. Dearnaley, J.H. Arps, Biomedical applications of diamond-like carbon (DLC) coatings: a review, *Surf. Coat. Technol.* 200 (2005) 2518–2524.

- [10] H.M. Mobarak, H.H. Masjuki, E.N. Mohamad, M.A. Kalam, H.K. Rashedul, M.M. Rashed, M. Habibullah, Tribological properties of amorphous hydrogenated (a-C:H) and hydrogen-free tetrahedral (ta-C) diamond-like carbon coatings under jatropa biodegradable lubricating oil at different temperatures, *Appl. Surf. Sci.* 317 (2014) 581–592.
- [11] X. Li, P. Guo, L. Sun, A. Wang, P. Ke, Ab initio investigation on Cu/Cr codoped amorphous carbon nanocomposite films with giant residual stress reduction, *ACS Appl. Mater. Interfaces* 7 (2015) 27878–27884.
- [12] X. Li, L. Sun, P. Guo, P. Ke, A. Wang, Structure and residual stress evolution of Ti/Al, Cr/Al or W/Al co-doped amorphous carbon nanocomposite films: insights from ab initio calculations, *Mater. Des.* 89 (2016) 1123–1129.
- [13] L. Sun, P. Guo, P. Ke, X. Li, A. Wang, Synergistic effect of Cu/Cr co-doping on the wettability and mechanical properties of diamond-like carbon films, *Diam. Relat. Mater.* 68 (2016) 1–9.
- [14] S. Zhou, L. Wang, S.C. Wang, Q. Xue, Comparative study of simplex doped nc-WC/a-C and duplex doped nc-WC/a-C(Al) nanocomposite coatings, *Appl. Surf. Sci.* 257 (2011) 6971–6979.
- [15] C. Kong, P. Guo, L. Sun, Y. Zhou, Y. Liang, X. Li, P. Ke, K.-R. Lee, A. Wang, Tribological mechanism of diamond-like carbon films induced by Ti/Al co-doping, *Surf. Coat. Technol.* 342 (2018) 167–177.
- [16] H. Song, L. Ji, H. Li, X. Liu, H. Zhou, L. Liu, J. Chen, Improving the tribological performance of a-C:H film in a high vacuum by surface texture, *J. Phys. D: Appl. Phys.* 47 (2014) 235301.
- [17] U. Pettersson, S. Jacobson, Influence of surface texture on boundary lubricated sliding contacts, *Tribol. Int.* 36 (2003) 857–864.
- [18] Y. Hu, H. Liu, X. Zhou, H. Pan, X. Wu, N. Abidi, Y. Zhu, J. Wang, Surface engineering of spongy bacterial cellulose via constructing crossed groove/column micropattern by low-energy CO<sub>2</sub> laser photolithography toward scar-free wound healing, *Mater. Sci. Eng. C Mater. Biol. Appl.* 99 (2019) 333–343.
- [19] X.L. Wang, K. Kato, K. Adachi, K. Aizawa, Loads carrying capacity map for the surface texture design of SiC thrust bearing sliding in water, *Tribol. Int.* 36 (2003) 189–197.
- [20] Y. Aoki, N. Ohtake, Tribological properties of segment-structured diamond-like carbon films, *Tribol. Int.* 37 (2004) 941–947.
- [21] A. Arslan, H.H. Masjuki, M. Varman, M.A. Kalam, M.M. Quazi, K.A.H. Al Mahmud, M. Gulzar, M. Habibullah, Effects of texture diameter and depth on the tribological performance of DLC coating under lubricated sliding condition, *Appl. Surf. Sci.* 356 (2015) 1135–1149.
- [22] A. Ronen, I. Etsion, Y. Kligerman, Friction-Reducing Surface-Texturing in Reciprocating Automotive Components, *Tribol. Trans.* 44 (2001) 359–366.
- [23] V. Kashyap, P. Ramkumar, Feasibility study of micro-groove cross hatched surface texturing on Ti6Al4V for improved biotribological performance in metal-on-polymer hip implant, *Tribol.-Mater. Surf. Interfaces* 13 (2019) 150–160.
- [24] Z. Wu, Y. Xing, P. Huang, L. Liu, Tribological properties of dimple-textured titanium alloys under dry sliding contact, *Surf. Coat. Technol.* 309 (2017) 21–28.
- [25] T. Guo, C. Kong, X. Li, P. Guo, Z. Wang, A. Wang, Microstructure and mechanical properties of Ti/Al co-doped DLC films: dependence on sputtering current, source gas, and substrate bias, *Appl. Surf. Sci.* 410 (2017) 51–59.
- [26] X. Li, P. Guo, L. Sun, X. Zuo, D. Zhang, P. Ke, A. Wang, Ti/Al co-doping induced residual stress reduction and bond structure evolution of amorphous carbon films: an experimental and ab initio study, *Carbon* 111 (2017) 467–475.
- [27] Y. Zhou, P. Guo, L. Sun, L. Liu, X. Xu, W. Li, X. Li, K.-R. Lee, A. Wang, Microstructure and property evolution of diamond-like carbon films co-doped by Al and Ti with different ratios, *Surf. Coat. Technol.* 361 (2019) 83–90.
- [28] J. Pu, D. He, L. Wang, Effects of WC phase contents on the microstructure, mechanical properties and tribological behaviors of WC/a-C superlattice coatings, *Appl. Surf. Sci.* 357 (2015) 2039–2047.
- [29] L. Qiang, K. Gao, L. Zhang, J. Wang, B. Zhang, J. Zhang, Further improving the mechanical and tribological properties of low content Ti-doped DLC film by W incorporating, *Appl. Surf. Sci.* 353 (2015) 522–529.
- [30] S. Veprek, M.G.J. Veprek-Heijman, P. Karvankova, J. Prochazka, Different approaches to superhard coatings and nanocomposites, *Thin Solid Films* 476 (2005) 1–29.
- [31] N.A. Sakharova, J.V. Fernandes, M.C. Oliveira, J.M. Antunes, Influence of ductile interlayers on mechanical behaviour of hard coatings under depth-sensing indentation: a numerical study on TiAlN, *J. Mater. Sci.* 45 (2010) 3812–3823.
- [32] A. Amanov, T. Watabe, R. Tsuboi, S. Sasaki, Improvement in the tribological characteristics of Si-DLC coating by laser surface texturing under oil-lubricated point contacts at various temperatures, *Surf. Coat. Technol.* 232 (2013) 549–560.
- [33] P.W. Shum, Z.F. Zhou, K.Y. Li, Investigation of the tribological properties of the different textured DLC coatings under reciprocating lubricated conditions, *Tribol. Int.* 65 (2013) 259–264.
- [34] F. Ali, M. Kaneta, I. Křupka, M. Hartl, Experimental and numerical investigation on the behavior of transverse limited micro-grooves in EHL point contacts, *Tribol. Int.* 84 (2015) 81–89.
- [35] F.S. Boi, X. Zhang, D. Medranda, Evidence of sp<sup>3</sup>-rich nano-diamond-like characteristics in amorphous carbon foam continuously filled with α-Fe, *Diam. Relat. Mater.* 84 (2018) 190–195.
- [36] Y.J. Jo, T.F. Zhang, M.J. Son, K.H. Kim, Synthesis and electrochemical properties of Ti-doped DLC films by a hybrid PVD/PECVD process, *Appl. Surf. Sci.* 433 (2018) 1184–1191.
- [37] Y. Ye, C. Wang, Y. Wang, W. Zhao, J. Li, Y. Yao, A novel strategy to enhance the tribological properties of Cr/GLC films in seawater by surface texturing, *Surf. Coat. Technol.* 280 (2015) 338–346.
- [38] D. He, S. Zheng, J. Pu, G. Zhang, L. Hu, Improving tribological properties of titanium alloys by combining laser surface texturing and diamond-like carbon film, *Tribol. Int.* 82 (2015) 20–27.